IEEE Access
Multidisciplinary : Rapid Review : Open Access Journal

Received September 18, 2017, accepted December 14, 2017, date of publication December 22, 2017,
date of current version March 9, 2018.

Digital Object Identifier 10.1109/ACCESS.2017.2786472

Design of a High-Isolation n-Way Power Combiner Based on a 2n + 1 Port Mode Network

LETIAN GUO, JIAWEI LI, WENHUA HUANG, HAO SHAO, AND TAO BA
Science and Technology on High Power Microwave Laboratory, Northwest Institute of Nuclear Technology, Xi'an 710024, China

Corresponding author: Letian Guo (guoletian19901230@126.com)

ABSTRACT This paper proposes a design method for high-isolation n-way power combiners based on 2n + 1 port mode networks. The scattering matrix of a 2n + 1 port mode network is obtained by rigorously deriving the voltage and current relations. Following the proposed method, a compact four-way coaxial power combiner based on a nine-port mode network is designed and fabricated. Measurements show that from 7.8 to 10.3 GHz, the return losses of the input and output ports are better than −18 and −21 dB, respectively, the isolation levels between the input ports are higher than 21 dB, the insertion loss for power combination is less than 0.2 dB, and the amplitude and phase imbalances of the power combiner are less than approximately 0.15 dB and 2°, respectively. The simulated results agree well with the measured results. Moreover, the combiner has compact cross-sectional dimensions of $1.2\lambda \times 1.2\lambda$. It is clear that the designed four-way power combiner is superior in terms of its compact cross-sectional dimensions, high degree of isolation, low return loss, low insertion loss, and output amplitude and phase imbalance, which make it well suited for solid-state power combination. In addition, the power combiner is easy to fabricate and assemble. The proposed method shows great potential for realizing multi-way power combination with high isolation, low return loss, and compact cross-sectional dimensions.

INDEX TERMS High isolation, mode network, power combiner.

I. INTRODUCTION

HIGH-EFFICIENCY, high-power microwave and millimeter-wave solid-state amplifiers have been extensively implemented in many systems [1], and power combiners have been widely investigated and developed to improve the output power of solid-state devices [2]–[31]. An ideal power divider-combiner exhibits low insertion losses, low return losses, a high degree of isolation, and a broad fractional bandwidth. In this paper, we propose a universal circuit model for n-way power combination based on a 2n + 1 port mode network. This model can achieve nearly all of the ideal characteristics of a power combiner. The power combiners thus designed are intended to be used to combine kW-level signals from several individual amplifiers to feed the antenna elements that constitute an active antenna array. In the case of such a power combiner, several other issues must also be considered, such as its power capacity, which must be sufficient to transmit several kW, and its cross-sectional surface area, which influences the antenna size and determines the beam scanning range of the array.

Several types of multi-way power combiners have previously been studied, such as traveling-wave power combiners [7]–[16], radial power combiners [17]–[25], and binary power combiners [26], [27]. Among these devices, conventional traveling-wave power dividers and radial coaxial power dividers can satisfy the requirements of broad bandwidth, high power capacity, low insertion loss, and potentially compact volume. By contrast, conventional binary waveguide power dividers are typically bulky, and consequently, their applications are very limited. In addition, for all three types of power combiners, it is difficult to achieve a high degree of isolation and low return losses at the output ports while simultaneously maintaining a high power capacity [28]–[37].

In this paper, a novel universal circuit model for achieving high-isolation n-way power combination based on a 2n + 1 port mode network is proposed and analyzed. In accordance with the proposed circuit model, a 4-way coaxial power combiner based on a 9-port coaxial mode network is designed to validate our method.

II. DESIGN OF AN N-WAY POWER COMBINER BASED ON A 2*N* + 1 PORT MODE NETWORK

In this paper, we propose a universal method for designing an n-way power combiner with inherently high isolation and low return loss [32]. The designed n-way power combiner is based on a 2n + 1 port mode network, which is composed of

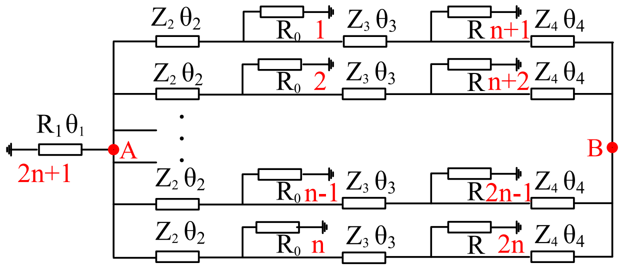

FIGURE 1. The circuit pattern of an n-way power combiner based on a 2n + 1 port mode network.

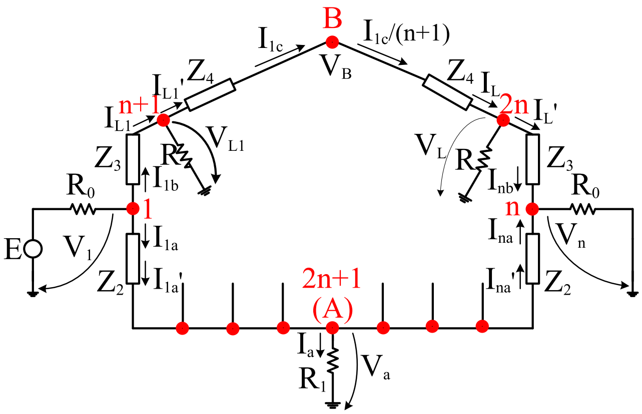

FIGURE 2. The voltage-current distribution pattern of the n-way power combiner when input port 1 is excited.

multi-section ideal TEM transmission lines. The corresponding circuit model is shown in Fig. 1. The input ports and matched ports of the n-way power combiner are numbered 1, 2, ..., n and n + 1, n + 2 ..., 2n, respectively. The output port of the n-way power combiner is numbered as port 2n+1. The characteristic impedances of the input ports, matched ports, and output port are denoted by R_0, R, and R_1. We assume that R_0, R, and R_1 are purely resistive. The characteristic impedances of the three types of interconnected transmission lines are denoted by Z_2, Z_3, and Z_4. Their corresponding lengths are denoted by θ_2, θ_3, and θ_4, respectively. A and B are both common electrical connection nodes. In this section, we first investigate the circuit pattern and derive the necessary conditions to achieve high isolation and perfect matching. Then, through a systematic analysis of the n-way power division, all elements of the scattering matrix of the 2n + 1 port mode network are derived.

A. CONDITIONS FOR HIGH ISOLATION AND PERFECT MATCHING

Regarding the ideal transmission line circuit model, we consider the circuit to be reciprocal and non-lossy. To simplify the analysis, we consider all connection lines to have a length of one quarter wavelength; thus, $\theta_2 = \theta_3 = \theta_4 = 90°$. When input port 1 is excited, the voltage-current distribution pattern dictated by the circumferential symmetry is as illustrated in Fig. 2.

The transfer matrix for one transmission-line section, with a characteristic impedance of Z_c and a length of 90°, can be written as follows:

$$\begin{bmatrix} 0 & jZ_c \\ \frac{j}{Z_c} & 0 \end{bmatrix}$$

According to the voltage-current relation for Z_2 near port 1, we can obtain (1):

$$\begin{bmatrix} V_1 \\ I_{1a} \end{bmatrix} = \begin{bmatrix} 0 & jZ_2 \\ \frac{j}{Z_2} & 0 \end{bmatrix} \begin{bmatrix} V_a \\ I'_{1a} \end{bmatrix} \tag{1}$$

From (1), we can easily obtain (2a) and (2b):

$$V_1 = jZ_2 I'_{1a} \tag{2a}$$

$$I_{1a} = \frac{j}{Z_2} V_a \tag{2b}$$

Similarly, according to the voltage-current relation for Z_n near port n, we can obtain (4a), (4a), and (4b):

$$\begin{bmatrix} V_a \\ I'_{na} \end{bmatrix} = \begin{bmatrix} 0 & jZ_2 \\ \frac{j}{Z_2} & 0 \end{bmatrix} \begin{bmatrix} V_n \\ I_{na} \end{bmatrix} \tag{3}$$

$$V_a = jZ_2 I_{na} \tag{4a}$$

$$I'_{na} = \frac{j}{Z_2} V_n \tag{4b}$$

From the symmetry of the structure, considering the voltage-current relation for node A, we can obtain (5):

$$I'_{1a} = \frac{V_a}{R_1} + (n-1) I'_{na} \tag{5}$$

Similarly, we can obtain (6a) and (6b) from the voltage-current relations for ports 1 and n:

$$I_{na} = \frac{V_n}{R_0} - I_{nb} \tag{6a}$$

$$I_{1a} = \frac{E - V_1}{R_0} - I_{1b} \tag{6b}$$

By substituting (4b) and (5) into (2a), substituting (6a) into (4a), and substituting (6b) into (2b), we obtain (7)-(9):

$$V_1 = jZ_2 [\frac{V_a}{R_1} + (n-1) j \frac{V_n}{Z_2}] \tag{7}$$

$$V_a = jZ_2 [\frac{V_n}{R_0} - I_{nb}] \tag{8}$$

$$j\frac{V_a}{Z_2} = \frac{E - V_1}{R_0} - I_{1b} \tag{9}$$

To express the currents I_{1b} and I_{nb} in terms of the voltages V_1, V_n, and V_a, we use the transfer matrix to express the relations between the voltages and currents on the right side of the circuit pattern from node B to port n as follows:

$$\begin{bmatrix} V_B \\ \frac{I_{1c}}{n-1} \end{bmatrix} = \begin{bmatrix} 0 & jZ_4 \\ \frac{j}{Z_4} & 0 \end{bmatrix} [\begin{matrix} V_L \\ I_L \end{matrix}] \tag{10}$$

$$\begin{bmatrix} V_L \\ I_L \end{bmatrix} = \begin{bmatrix} 1 & 0 \\ \frac{1}{R} & 1 \end{bmatrix} \begin{bmatrix} V_L \\ I'_L \end{bmatrix} \tag{11}$$

$$\begin{bmatrix} V_L \\ I'_L \end{bmatrix} = \begin{bmatrix} 0 & jZ_3 \\ \frac{j}{Z_3} & 0 \end{bmatrix} \begin{bmatrix} V_n \\ I_{nb} \end{bmatrix} \tag{12}$$

By cascading (10)-(12), we obtain (13):

$$\begin{bmatrix} V_B \\ I_{1c} \end{bmatrix} = \begin{bmatrix} -\frac{Z_4}{Z_3} & \frac{-Z_3Z_4}{R} \\ 0 & -\frac{Z_3}{Z_4}(n-1) \end{bmatrix} \begin{bmatrix} V_n \\ I_{nb} \end{bmatrix} \tag{13}$$

Similarly, for the left side of the circuit pattern from port 1 to node B, we obtain (14):

$$\begin{bmatrix} V_1 \\ I_{1b} \end{bmatrix} = \begin{bmatrix} -\frac{Z_3}{Z_4} & \frac{-Z_3Z_4}{R} \\ 0 & -\frac{Z_4}{Z_3} \end{bmatrix} \begin{bmatrix} V_B \\ I_{1c} \end{bmatrix} \tag{14}$$

By substituting (14) into (13), we derive (15):

$$\begin{bmatrix} V_1 \\ I_{1b} \end{bmatrix} = \begin{bmatrix} 1 & \frac{nZ_3^2}{R} \\ 0 & n-1 \end{bmatrix} \begin{bmatrix} V_n \\ I_{nb} \end{bmatrix} \tag{15}$$

By solving (15), we obtain (16) and (17):

$$I_{nb} = \frac{(V_1 - V_n)R}{nZ_3^2} \tag{16}$$

$$I_{1b} = \frac{n-1}{n}\frac{(V_1 - V_n)R}{Z_3^2} \tag{17}$$

Upon simplifying (7), substituting (16) into (8), and substituting (17) into (9), we obtain (18)-(20):

$$V_1 = jV_a\frac{Z_2}{R_1} - (n-1)V_n \tag{18}$$

$$V_a = jV_n\frac{Z_2}{R_0} - j\frac{Z_2R}{nZ_3^2}(V_1 - V_n) \tag{19}$$

$$\frac{E - V_1}{R_0} = j\frac{V_a}{Z_2} + \frac{n-1}{n}\frac{R}{Z_3^2}(V_1 - V_n) \tag{20}$$

To achieve high isolation, V_n must be equal to 0 when an input port is excited. Moreover, for perfect matching of the input port, the condition $E = 2V_1$ should also be met. Upon substituting these two conditions into (18)-(20), we obtain

$$V_1 = jV_a\frac{Z_2}{R_1} \tag{21}$$

$$jV_a = \frac{Z_2R}{nZ_3^2}V_1 \tag{22}$$

$$V_1 = jV_a\frac{R_0}{Z_2} + \frac{n-1}{n}\frac{RR_0V_1}{Z_3^2} \tag{23}$$

By simplifying (21)-(23), we obtain (24) and (25):

$$\frac{Z_2R}{nZ_3^2} = \frac{R_1}{Z_2} \tag{24}$$

$$1 = \frac{R_0R_1}{Z_2^2} + \frac{n-1}{n}\frac{RR_0}{Z_3^2} \tag{25}$$

Then, by solving (24) and (25), we obtain (26) and (27). Thus, the two fundamental conditions for perfect matching and high isolation are derived.

$$Z_3 = \sqrt{RR_0} \tag{26}$$

$$Z_2 = \sqrt{nR_1R_0} \tag{27}$$

B. ANALYSIS OF THE SCATTERING MATRIX OF AN N-WAY POWER COMBINER BASED ON A 2N + 1 PORT MODE NETWORK

To more clearly understand the combination mechanism and validate the combination conditions, the scattering matrix of an n-way power combiner based on a 2n + 1 port mode network is derived in this subsection. First, we solve for the voltages at all ports when port 1 is excited. Then, we compute the power coupled to these ports and derive the corresponding S-parameters.

Port 1 is perfectly matched, so the power excited at port 1 can be computed as shown in (28):

$$P_{in} = \frac{|V_1|^2}{R_0} \tag{28}$$

By substituting $V_{\rm n} = 0$ into (19), we can obtain the output voltage and power at port 2n + 1, as shown in (29) and (30):

$$V_a = jZ_2\frac{V_1R}{nZ_3^2} \tag{29}$$

$$P_{out} = \frac{V_aV_a^*}{R_1} = \frac{1}{n}\frac{|V_1|^2}{R_0} \tag{30}$$

Similarly, the voltages at ports n + 2, n + 3, . . . , 2n and port n + 1 are expressed by (31) and (32), respectively.

$$V_L = jZ_3I_{nb} = \frac{j(V_1 - V_n)R}{nZ_3} = \frac{jV_1R}{nZ_3} \tag{31}$$

$$V_{L1} = -jZ_3I_{1b} = -j\frac{n-1}{n}\frac{V_1R}{Z_3} \tag{32}$$

Thus, the output power at ports n + 2, n + 3, . . . , 2n and port n + 1 can be computed as shown in (33) and (34), respectively.

$$P_L = \frac{V_LV_L^*}{R} = \frac{1}{n^2}\frac{|V_1|^2R}{Z_3^2} \tag{33}$$

$$P_{L1} = \frac{V_{L1}V_{L1}^*}{R} = \left(\frac{n-1}{n}\right)^2\frac{|V_1|^2R}{Z_3^2} \tag{34}$$

Finally, we obtain

$$S_{1,m} = 0 \quad m = 1, 2 \ldots n \tag{35a}$$

$$|S_{1,n+1}| = \frac{n-1}{n} \tag{35b}$$

$$|S_{1,m}| = \frac{1}{n} \quad m = n+2, \ldots 2n \tag{35c}$$

$$|S_{1,2n+1}| = \frac{1}{\sqrt{n}} \tag{35d}$$

Considering the symmetry of the structure, (35a)-(35d) can be expanded to obtain (36a)-(36f).

$$S_{m',m} = 0 \quad m' = 1, \ldots n \; m = 1, \ldots n \tag{36a}$$

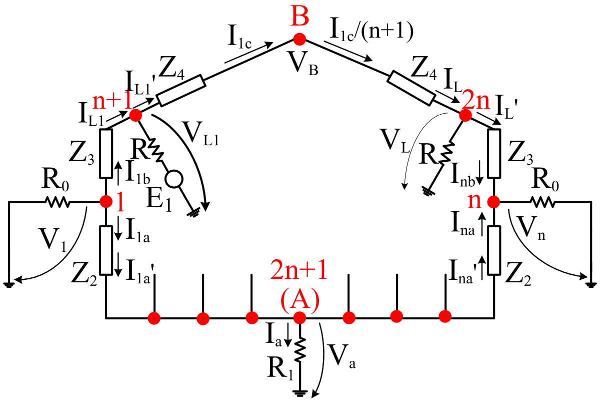

FIGURE 3. The voltage-current distribution pattern of an n-way power combiner when input port n + 1 is excited.

$$\left|S_{m',n+m'}\right| = \frac{n-1}{n} \quad m' = 1, 2, 3 \ldots .n \tag{36b}$$

$$\left|S_{m',m}\right| = \frac{1}{n} \quad m' = 2, 3 \ldots .n \; m = n+1, \ldots .n+m'-1 \; \&n+m'+1 \ldots \ldots .2n \tag{36c}$$

$$\left|S_{1,m}\right| = \frac{1}{n} \quad m = n+2, \ldots .2n \tag{36d}$$

$$\left|S_{m',2n+1}\right| = \frac{1}{\sqrt{n}} \quad m' = 1, 2, \ldots n \tag{36e}$$

Thus, the coupling relations between one input port and all other ports are obtained. Now, to obtain the solution for the entire scattering matrix, we also need to analyze the coupling relations when one matching port is excited. The voltage-current distribution pattern when only matching port n + 1 is excited is shown in Fig. 3.

From the reciprocal, non-lossy, and orthogonal characteristics of the system, it is easy to obtain (37). This equation expresses that when any matching port is excited, there is no power output at the output port of the combiner, port 2n + 1. Thus, (38) is obtained as follows.

$$\left|S_{m',2n+1}\right| = 0 \quad m' = n+1, n+2, \ldots 2n \tag{37}$$

$$V_a = 0 \tag{38}$$

Equation (8) also holds for the circuit pattern in Fig. 3. Substituting (38) into (8), we obtain (39).

$$I_{nb} = \frac{V_n}{R_0} \tag{39}$$

For Fig. 3, in accordance with the transfer-matrix relation from Z_4 on the left side to Z_3 on the right side, we can obtain (40).

$$\begin{bmatrix} V_{L1} \\ I'_{L1} \end{bmatrix} = \begin{bmatrix} 0 & jZ_4 \\ \frac{j}{Z_4} & 0 \end{bmatrix} \begin{bmatrix} 0 & jZ_4 \\ \frac{j}{Z_4} & 0 \end{bmatrix} \begin{bmatrix} 1 & 0 \\ \frac{1}{R} & 1 \end{bmatrix} \begin{bmatrix} 0 & jZ_3 \\ \frac{j}{Z_3} & 0 \end{bmatrix} * \begin{bmatrix} V_n \\ I_{nb} \end{bmatrix} = \begin{bmatrix} 0 & -j(n-1)Z_3 \\ \frac{-j}{Z_3} & \frac{-j(n-1)Z_3}{Z_4} \end{bmatrix} \begin{bmatrix} V_n \\ I_{nb} \end{bmatrix} \tag{40}$$

Considering (39) and (40), we can easily obtain (41)-(43):

$$I_{nb} = \frac{jV_{L1}}{(n-1)Z_3} \tag{41}$$

$$V_n = \frac{jV_{L1}}{n-1}\frac{R_0}{Z_3} \tag{42}$$

$$I'_{L1} = \frac{-j}{Z_3}V_n + \frac{-jZ_3}{R}I_{nb} = \frac{2V_{L1}}{(n-1)R} \tag{43}$$

Similarly, in accordance with the transfer-matrix relation from node A to port n + 1 on the left side in Fig. 3, we can obtain (44):

$$\begin{bmatrix} V_a \\ -I_{1a'} \end{bmatrix} = \begin{bmatrix} -\frac{Z_4}{Z_3} & \frac{-Z_2Z_3}{R_0} \\ 0 & \frac{-Z_3}{Z_2} \end{bmatrix} \begin{bmatrix} V_{L1} \\ I_{L1} \end{bmatrix} \tag{44}$$

From (44) and considering (26), (27), and (38), we can obtain (45):

$$I_{L1} = -\frac{V_{L1}}{R} \tag{45}$$

From the current relation at port n + 1, we can obtain (47):

$$\frac{E - V_{L1}}{R} = -I_{L1} + I'_{L1} \tag{46}$$

By substituting (43) and (45) into (46), we obtain (47) and (48):

$$\frac{E - V_{L1}}{R} = \frac{(n+1)}{(n-1)}\frac{V_{L1}}{R} \tag{47}$$

$$E = \frac{2n}{n-1}V_{L1} \tag{48}$$

The voltages at the other matching ports can also be easily derived, as shown in (49):

$$V_L = jZ_3 I_{nb} = -\frac{V_{L1}}{n-1} \tag{49}$$

Z_F is defined as the input impedance seen from the excited matching port n + 1. We can thus derive (50) in terms of Z_F.

$$\frac{R}{Z_F} = \frac{E - V_{L1}}{V_{L1}} = \frac{n+1}{n-1} \tag{50}$$

Γ denotes the reflection at the excited port n + 1 and is expressed as shown in (51). V^+ is the forward incident voltage at the excited port n + 1 and is given in (52). Considering (49) and (52), we can easily obtain (53) and (54). P_{in} is the incident power at the excited port n + 1, and P_{others} is the power coupled to the other matching ports.

$$\Gamma = \frac{Z_F - R}{Z_F + R} = -\frac{1}{n} \tag{51}$$

$$V^+ = \frac{V_{L1}}{1+\Gamma} = \frac{n}{n-1}V_{L1} \tag{52}$$

$$P_{in} = \frac{V^+(V^+)^*}{R} = \frac{n^2}{(n-1)^2}\frac{|V_{L1}|^2}{R} \tag{53}$$

$$P_{others} = \frac{V_L V_L^*}{R} = \frac{1}{(n-1)^2}\frac{|V_{L1}|^2}{R} \tag{54}$$

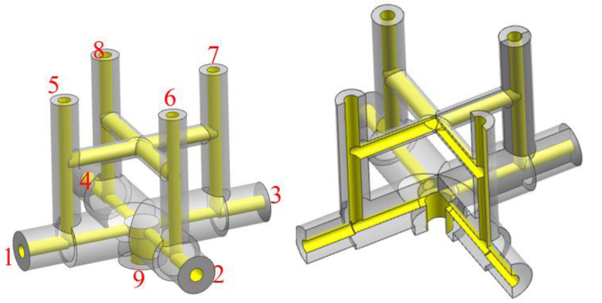

(a) (b)

FIGURE 4. The 4-way coaxial power combiner: (a) the entire structure; (b) a sectional view of the structure (the red numbers 1-9 indicate the 9 ports of the power combiner, the yellow structure represents the inner conductor of the vacuum coaxial waveguides, and the gray structures represent the vacuum portions of the vacuum coaxial waveguides).

From (51), (53), and (54) and considering the symmetry of the structure, we can obtain (55):

$$|S_{m',m}| = \frac{1}{n} \quad m' = n+1, \ldots\ldots 2n \; m = n+1, \ldots\ldots 2n \tag{55}$$

Thus, by combining (36a)-(36e) and (55), the entire $(2n+1) \times (2n+1)$ scattering matrix of the n-way power combiner is obtained.

III. DESIGN OF A 4-WAY COAXIAL POWER COMBINER BASED ON THE PROPOSED METHOD

A. BASIC DESIGN OF THE 4-WAY POWER COMBINER

To validate the proposed circuit model, we designed a 4-way power combiner based on a 9-port mode network. To achieve high combination efficiency, vacuum coaxial waveguide transmission lines were used to construct the power divider. The design process can be summarized as follows:

1. According to the circuit model and the conditions for high isolation and perfect matching, we chose arbitrary initial impedance values for the ports and transmission lines.
   The initial lengths of the transmission lines were set equal to one quarter of the wavelength.
2. We used the ANSYS HFSS simulation software to easily build an initial model, with some consideration of the fabrication feasibility.
3. Through a brief optimization process, an excellent 4-way power combiner was obtained. The optimization was performed using the Sequential Non-linear Programming optimizer in HFSS. The objective function for optimization was defined as follows:

$$\begin{aligned}\delta = &(1+C_1)|S_{11}|^2 + (1+C_2)|S_{99}|^2 + (1+C_3)|S_{12}|^2 \\ &+ (1+C_4)|S_{13}|^2 + (1+C_5)|S_{95}|^2 + (1+C_6)| \\ &\times |S_{91}| - 0.5|^2 \to 0\end{aligned} \tag{56}$$

The frequency range for which the performance was to be optimized was set to 7.5–10.5 GHz. The values of the weight coefficients C_1–C_5 were initially set to 0 and were subsequently adjusted during the optimization process. The detailed structure and optimized S-parameters of the 4-way power combiner are shown in Figs. 4 and 5. According to the analysis presented in Section II, the scattering matrix

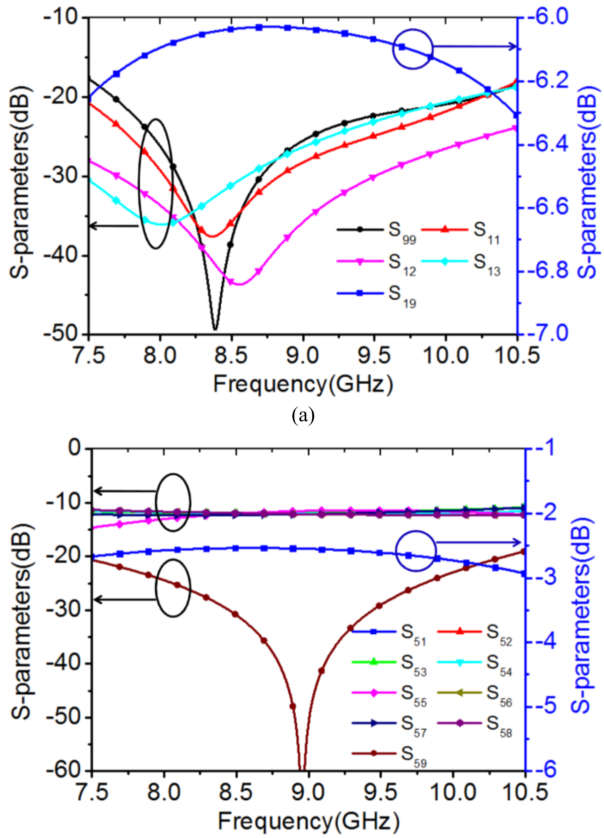

(b)

FIGURE 5. The optimized S-parameters of the 4-way coaxial power combiner: (a) S_{99}, S_{11}, S_{12}, S_{13}, and S_{19}; (b) S_{51}, S_{52}, S_{53}, S_{54}, S_{55}, S_{56}, S_{57}, S_{58}, and S_{59}.

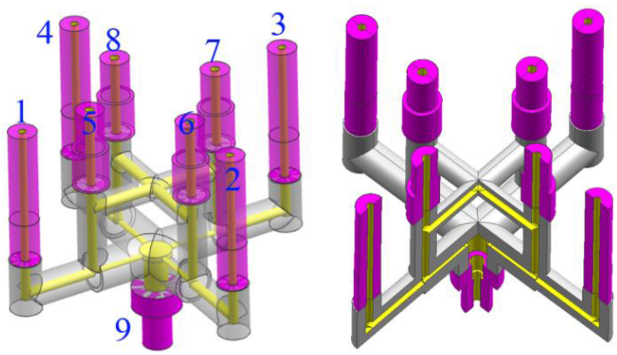

(a) (b)

FIGURE 6. The improved 4-way coaxial power combiner: (a) the entire structure; (b) a sectional view of the structure (the blue numbers 1-9 indicate the 9 ports of the power combiner, the yellow structure represents the inner conductor of the coaxial waveguides, the gray structures represent the vacuum portions of the coaxial waveguides, and the magenta structures represent the dielectric portions of the coaxial waveguides).

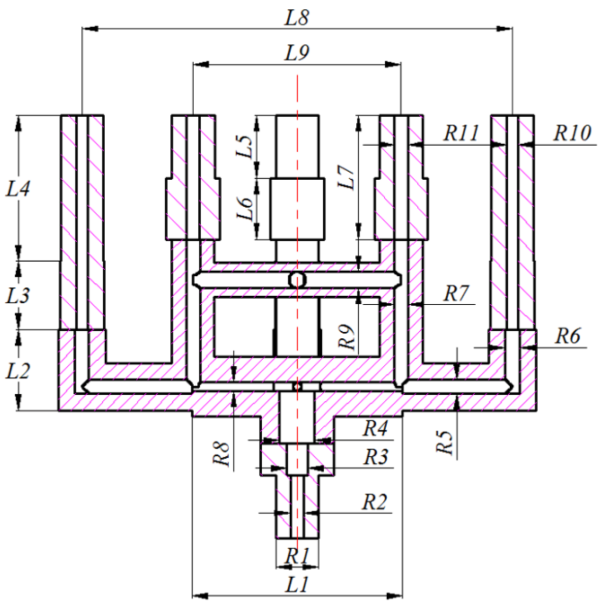

(a)

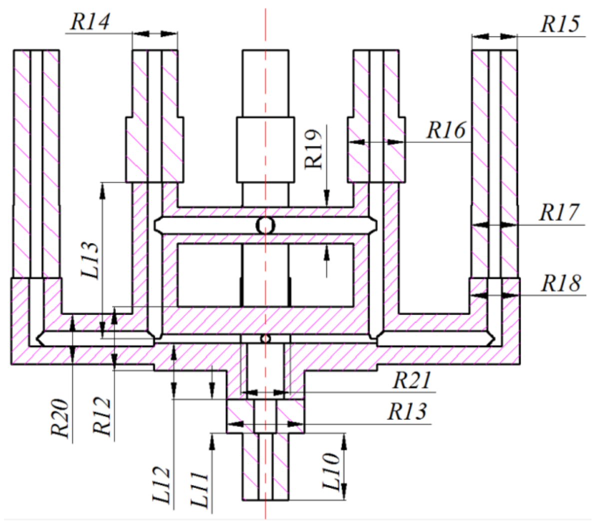

(b)

FIGURE 7. Final dimensions of the improved 4-way coaxial power combiner: (a) Part 1 of the final dimensions; (b) Part 2 of the final dimensions (the forward slashed areas represent vacuum coaxial waveguides, and the backward slashed areas represent dielectric coaxial waveguides).

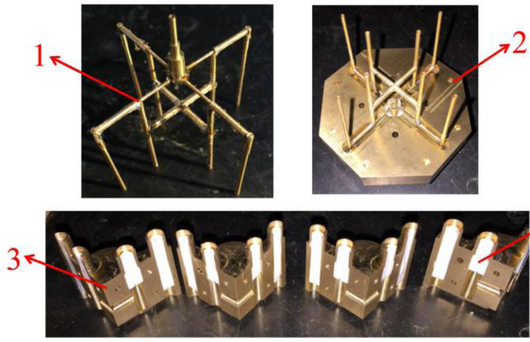

FIGURE 8. Sketch and assembly photographs of the 4-way coaxial power combiner (1-the welded inner conductor, 2-the outer metal shell close to the output port, 3-the outer metal shells close to the input ports, 4-the Teflon medium).

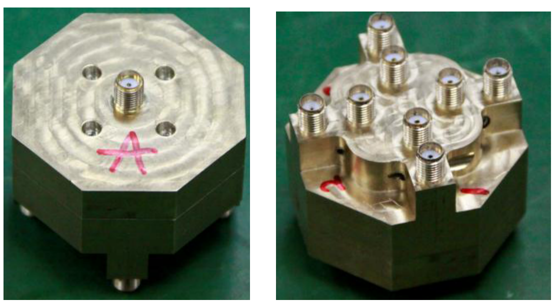

(a) (b)

FIGURE 9. Photographs of the fabricated power combiner: (a) top view; (b) bottom view.

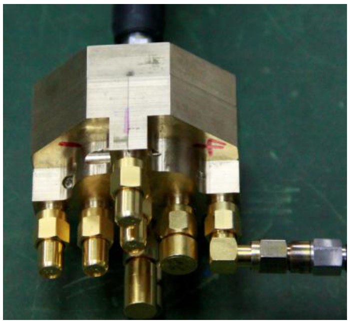

FIGURE 10. Measurement configuration of the power combiner.

of the 4-way power combiner can be written as shown in (57).

From 7.8 to 10.2 GHz, S_{11}, S_{12}, S_{13}, S_{59}, and S_{99} are less than −20 dB and thus correspond to the "0" element in (57); S_{19} is approximately −6 dB, which corresponds to the "1/2" element in (57); S_{51} is approximately −2.5 dB, which corresponds to the "3/4" element in (58); and S_{52}, S_{53}, S_{54}, S_{55}, S_{56}, S_{57}, and S_{58} are approximately −12 dB, which corresponds to the "1/4" element in (57). Considering the symmetry of the structure, the S-parameters of the 4-way coaxial power combiner are consistent with (57). Thus, the theory presented in Section II is well validated.

B. ENGINEERING REALIZATION OF THE 4-WAY POWER COMBINER

To reduce the cross-sectional dimensions of the power combiner, input ports 1-4 were set to lie in same directions as matched ports 5-8 with 90° coaxial bends. Notably, from the fabrication perspective, the 4-way power combiner should not be composed solely of vacuum coaxial waveguides because the inner conductors of vacuum coaxial waveguides cannot be mechanically fixed. Moreover, for convenience in measurement, it is preferable for the ports to taper to 50 Ω standard connectors. Thus, all ports were tapered to 50 Ω standard ports by means of dielectric coaxial matching waveguides

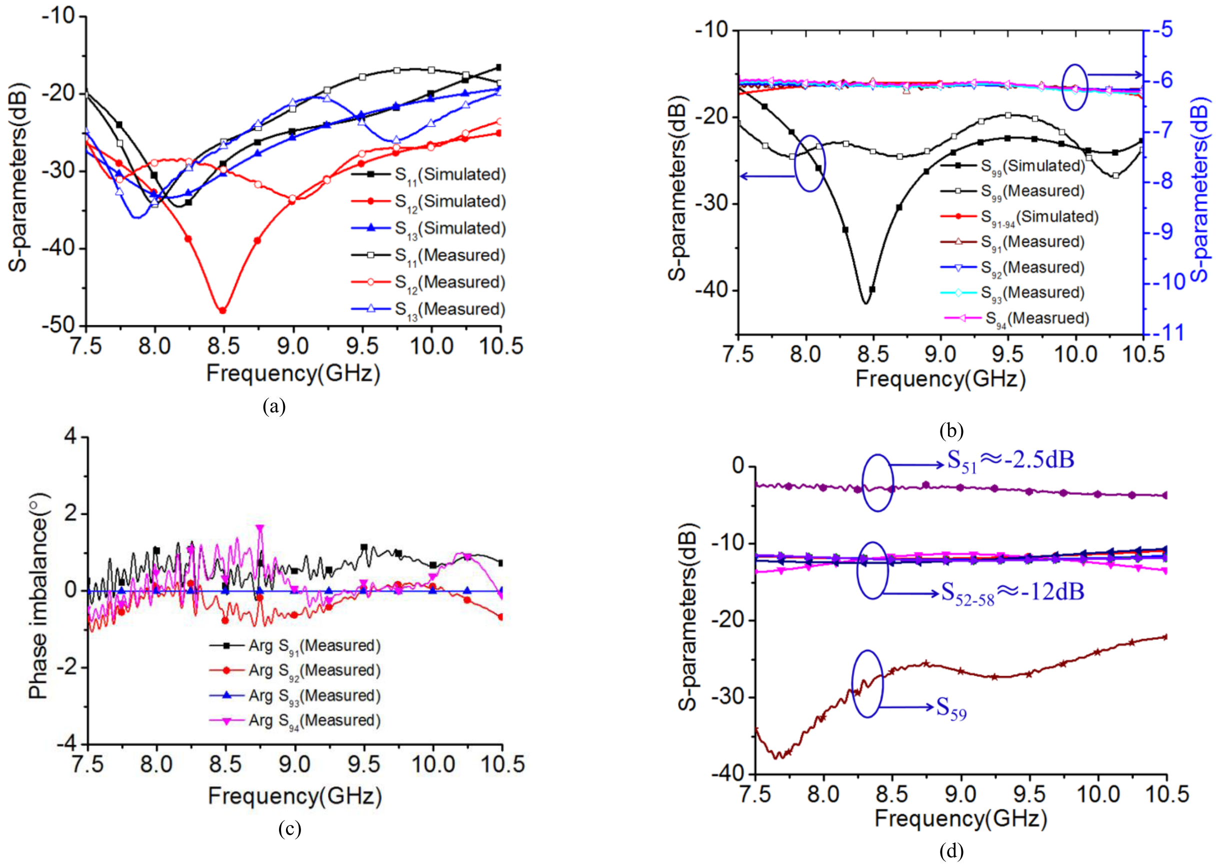

FIGURE 11. **The simulated and measured results for the 4-way coaxial power combiner: (a) S_{11}, S_{12}, and S_{13}; (b) S_{99}, S_{91}, S_{92}, S_{93}, and S_{94}; (c) phase imbalance; (d) measured values of S_{51}, S_{52}, S_{53}, S_{54}, S_{55}, S_{56}, S_{57}, S_{58}, and S_{59}.**

to facilitate fabrication and measurement. The corresponding improved power combiner design is illustrated in Fig. 6.

The final optimized dimensions of the 4-way power combiner, as labeled in Fig. 7, are $R_1 = 4.10$ mm, $R_2 = 1.27$ mm, $R_3 = 2.01$ mm, $R_4 = 3.37$ mm, $R_5 = 1.35$ mm, $R_6 = 1.35$ mm, $R_7 = 1.30$ mm, $R_8 = 0.80$ mm, $R_9 = 1.57$ mm, $R_{10} = 1.10$ mm, $R_{11} = 1.27$ mm, $R_{12} = 5.69$ mm, $R_{13} = 7$ mm, $R_{14} = 4.10$ mm, $R_{15} = 4.10$ mm, $R_{16} = 5.14$ mm, $R_{17} = 4.18$ mm, $R_{18} = 4.52$ mm, $R_{19} = 3.30$ mm, $R_{20} = 4.52$ mm, $L_1 = 20.10$ mm, $L_2 = 7.71$ mm, $L_3 = 6.51$ mm, $L_4 = 13.92$ mm, $L_5 = 6.00$ mm, $L_6 = 5.85$ mm, $L_7 = 11.85$ mm, $L_8 = 41.17$ mm, $L_9 = 19.90$ mm, $L_{10} = 6.00$ mm, $L_{11} = 3.07$ mm, $L_{12} = 5.02$ mm, and $L_{13} = 14.03$ mm.

$$|S| = \frac{1}{4}\begin{bmatrix} 0 & 0 & 0 & 0 & 3 & 1 & 1 & 1 & 2 \\ 0 & 0 & 0 & 0 & 1 & 3 & 1 & 1 & 2 \\ 0 & 0 & 0 & 0 & 1 & 1 & 3 & 1 & 2 \\ 0 & 0 & 0 & 0 & 1 & 1 & 1 & 3 & 2 \\ 3 & 1 & 1 & 1 & 1 & 1 & 1 & 1 & 0 \\ 1 & 3 & 1 & 1 & 1 & 1 & 1 & 1 & 0 \\ 1 & 1 & 3 & 1 & 1 & 1 & 1 & 1 & 0 \\ 1 & 1 & 1 & 3 & 1 & 1 & 1 & 1 & 0 \\ 2 & 2 & 2 & 2 & 0 & 0 & 0 & 0 & 0 \end{bmatrix} \tag{57}$$

IV. FABRICATION AND MEASUREMENTS OF THE 4-WAY COAXIAL POWER COMBINER

The 4-way coaxial power combiner designed in the previous section was fabricated and measured. During the fabrication process, the structure was divided into three components: the inner conductor, the outer metal shells, and the Teflon medium. The inner conductor was constructed by welding together several copper cylinders with the appropriate radii. The outer metal shells were milled from various copper blocks using numerical control machines. The Teflon medium was milled from various Teflon blocks. These three main components were assembled with various copper bolts. The Teflon medium helped to maintain the precise positioning and mechanical fixation of the inner conductor at the 9 ports. In this way, the 4-way coaxial power combiner could be easily fabricated and assembled at low cost. The main components and the entire structure are depicted in Figs. 8 and 9, respectively.

Measurements were conducted using an HP8510C Vector Network Analyzer [37]–[41]. The experimental setup is illustrated in Fig. 10. The simulated and measured results are presented in Fig. 11.

As shown in Fig. 11, from 7.8 to 10.3 GHz, the return loss S_{11} is better than -18 dB, whereas, the isolation levels S_{12}

TABLE 1. Comparison of 4-way power combiners.

Reference	Frequency bandwidth	Cross-sectional dimensions	Insertion loss	Isolation	Input port return loss	Output port return loss	Amplitude imbalance	Phase imbalance
[7]	50% (6.8-11.3 GHz)	$2\lambda \times 0.8\lambda$	0.5 dB	/	/	/	/	/
[9]	26% (1.9-2.5 GHz)	$2\lambda \times 0.8\lambda$	0.5 dB	/	/	-14 dB	0.25 dB	/
[10]	15% (9.3-10.8 GHz)	3 D	0.4 dB	20 dB	/	-15 dB	/	/
[11]	28% (32-39 GHz)	3 D	0.75 dB	10 dB	/	-15 dB	± 1 dB	±12°
[12]	30% (28-38 GHz)	3 D	0.92 dB	20 dB	-15 dB	-19 dB	± 1 dB	/
[14]	30% (4.3-5.6 GHz)	3 D	0.8 dB	4 dB	/	-14 dB	± 0.7 dB	±5°
[25]	90% (6-15 GHz)	$2.4\lambda \times 1.8\lambda$	1 dB	8 dB	/	-10 dB	0.5 dB	/
This work	28% (7.8-10.3 GHz)	$1.2\lambda \times 1.2\lambda$	0.2 dB	21 dB	-18 dB	-20 dB	0.15 dB	1.5°

and S_{13} are better than -25 dB and -21 dB, respectively. Moreover, the return loss S_{99} is less than -20 dB. The insertion loss for power division under the excitation of port 9 is less than 0.2 dB. The amplitude and phase imbalances for 4-way power division are less than approximately 0.15 dB and 2°, respectively. The small deteriorations in the return loss and isolation relative to the simulated values are most likely related to the milled fillets at the steps and corners. Moreover, any slight mismatch of the coaxial loads could also contribute to this deterioration. The insertion loss of 0.2 dB can be primarily attributed to ohmic conduction loss. The amplitude and phase imbalances may be due to misalignment of the coaxial probes and assembly errors, which would break the symmetry of the structure.

V. CONCLUSION

This paper proposes a design method for high-isolation n-way power combiners based on 2n + 1 port mode networks. The scattering matrix of a 2n + 1 port mode network is obtained by rigorously deriving the voltage and current relations. This method shows great potential for realizing multi-way power combination with high isolation and low return loss. Following the proposed method, a compact 4-way coaxial power combiner based on a 9-port mode network is designed, fabricated, and measured. The simulated results are consistent with the measured results. Comparisons with other power combiners reported in the literature are presented in Table 1. It is clear that the designed 4-way power combiner is superior in terms of its compact cross-sectional dimensions, high degree of isolation, low return loss, low insertion loss, and output amplitude and phase imbalance, which make it well suited for solid-state power combination. In addition, the component structures are easy to fabricate and assemble.

REFERENCES

[1] U. H. Gysel, "A new N-way power divider/combiner suitable for high-power applications," in *IEEE MTT-S Int. Microw. Symp. Dig.*, May 1975, pp. 116–118.

[2] Y. Wu, W. Sun, S. W. Leung, Y. Diao, K. H. Chan, and Y. M. Siu, "Single-layer microstrip high-directivity coupled-line coupler with tight coupling," *IEEE Trans. Microw. Theory Techn.*, vol. 61, no. 2, pp. 746–753, Feb. 2013.

[3] R. D. Beyers and D. I. L. de Villiers, "A general isolation network for N-way power combiners/dividers," in *IEEE MTT-S Int. Microw. Symp. Dig.*, Phoenix, AZ, USA, May 2015, pp. 1–4.

[4] Y. Wu, L. Jiao, Z. Zhuang, and Y. Liu, "The art of power dividing: A review for state-of-the-art planar power dividers," *China Commun.*, vol. 14, no. 5, pp. 1–16, May 2017.

[5] W. Feng, Q. Xue, and W. Che, "Compact planar magic-T based on the double-sided parallel-strip line and the slotline coupling," *IEEE Trans. Microw. Theory Techn.*, vol. 58, no. 11, pp. 2915–2923, Nov. 2010.

[6] W. Feng, H. Zhu, W. Che, and Q. Xue, "Wideband in-phase and out-of-phase balanced power dividing and combining networks," *IEEE Trans. Microw. Theory Techn.*, vol. 62, no. 5, pp. 1192–1202, May 2014.

[7] A. Sanada, K. Fukui, and S. Nogi, "A waveguide type power divider/combiner of double-ladder multiple-port structure," *IEEE Trans. Microw. Theory Techn.*, vol. 42, no. 7, pp. 1154–1161, Jul. 1994.

[8] A. Sanada, K. Fukui, S. Nogi, and M. Sanagi, "Traveling-wave microwave power divider composed of reflectionless dividing units," *IEEE Trans. Microw. Theory Techn.*, vol. 43, no. 1, pp. 14–20, Jan. 1995.

[9] J. P. Becker and A. M. Oudghiri, "A planar probe double ladder waveguide power divider," *IEEE Microw. Wireless Compon. Lett.*, vol. 15, no. 3, pp. 168–170, Mar. 2005.

[10] L. A. Li, B. J. Hilliard, J. R. Shafer, J. Daggett, E. J. Dickman, and J. P. Becker, "A planar compatible traveling-wave waveguide-based power divider/combiner," *IEEE Trans. Microw. Theory Techn.*, vol. 56, no. 8, pp. 1889–1898, Aug. 2008.

[11] Q.-X. Chu, Z.-Y. Kang, Q.-S. Wu, and D.-Y. Mo, "An in-phase output *Ka*-band traveling-wave power divider/combiner using double ridge-waveguide couplers," *IEEE Trans. Microw. Theory Techn.*, vol. 61, no. 9, pp. 3247–3253, Sep. 2013.

[12] Z.-Y. Kang, Q.-X. Chu, and Q.-S. Wu, "A *Ka*-band broadband traveling-wave power divider/combiner based on low-loss septum unsymmetrical E-plane T-junction series," in *IEEE MTT-S Int. Microw. Symp. Dig.*, Montreal, QC, Canada, Jun. 2012, pp. 17–22.

[13] S. R. Rengarajan and J. J. Lynch, "Design of a traveling-wave slot array power divider using the method of moments and a genetic algorithm," *IEEE Trans. Microw. Theory Techn.*, vol. 63, no. 12, pp. 3981–3987, Dec. 2015.

[14] K. Song, S. Hu, F. Zhang, and Y. Zhu, "Four-way chained quasi-planar power divider using rectangular coaxial waveguide," *IEEE Microw. Wireless Compon. Lett.*, vol. 25, no. 6, pp. 373–375, Jun. 2015.

[15] X. Jiang, S. C. Ortiz, and A. Mortazawi, "A Ka-band power amplifier based on the traveling-wave power-dividing/combining slotted-waveguide circuit," *IEEE Trans. Microw. Theory Techn.*, vol. 52, no. 2, pp. 633–639, Feb. 2004.

[16] K. Song, Y. Fan, and Z. He, "Broadband radial waveguide spatial combiner," *IEEE Microw. Wireless Compon. Lett.*, vol. 18, no. 2, pp. 73–75, Feb. 2008.

[17] K. Song and Q. Xue, "Planar probe coaxial-waveguide power combiner/divider," *IEEE Trans. Microw. Theory Techn.*, vol. 57, no. 11, pp. 2761–2767, Nov. 2009.

[18] K. Song and Q. Xue, "Ultra-wideband ring-cavity multiple-way parallel power divider," *IEEE Trans. Ind. Electron.*, vol. 60, no. 10, pp. 4737–4745, Oct. 2013.

[19] M. Amjadi and E. Jafari, "Design of a broadband eight-way coaxial waveguide power combiner," *IEEE Trans. Microw. Theory Techn.*, vol. 60, no. 1, pp. 39–45, Jan. 2012.

[20] R. D. Beyers and D. I. L. de Villiers, "A general impedance tapered transition for N-Way conical and coaxial combiners," *IEEE Trans. Microw. Theory Techn.*, vol. 64, no. 12, pp. 4482–4490, Dec. 2016.

[21] X. Shan and Z. Shen, "A suspended-substrate Ku-band symmetric radial power combiner," *IEEE Microw. Compon. Lett.*, vol. 21, no. 12, pp. 652–654, Dec. 2011.
[22] Y.-P. Hong, D. F. Kimball, P. M. Asbeck, J.-G. Yook, and L. E. Larson, "Single-ended and differential radial power combiners implemented with a compact broadband probe," *IEEE Trans. Microw. Theory Techn.*, vol. 58, no. 6, pp. 1565–1572, Jun. 2010.
[23] A. E. Fathy, S.-W. Lee, and D. Kalokitis, "A simplified design approach for radial power combiners," *IEEE Trans. Microw. Theory Techn.*, vol. 54, no. 1, pp. 247–255, Jan. 2006.
[24] Q.-X. Chu, D.-Y. Mo, and Q.-S. Wu, "An isolated radial power divider via circular waveguide TE_{01}-mode transducer," *IEEE Trans. Microw. Theory Techn.*, vol. 63, no. 12, pp. 3988–3996, Dec. 2015.
[25] M. Ahmadzadeh, P. Rasekh, R. Safian, G. Askari, and H. Mirmohammad-sadeghi, "Broadband rectangular high power divider/combiner," *IET Microw., Antennas Propag.*, vol. 9, no. 1, pp. 58–63, 2015.
[26] L. W. Epp, D. J. Hoppe, A. R. Khan, and S. L. Stride, "A high-power *Ka*-band (31–36 GHz) solid-state amplifier based on low-loss corporate waveguide combining," *IEEE Trans. Microw. Theory Techn.*, vol. 56, no. 8, pp. 1899–1908, Aug. 2008.
[27] Q. X. Chu, Q. S. Wu, and D. Y. Mo, "A *Ka*-band *E*-plane waveguide magic-T with coplanar arms," *IEEE Trans. Microw. Theory Techn.*, vol. 62, no. 11, pp. 2673–2679, Nov. 2014.
[28] X. Shan and Z. Shen, "An eight-way power combiner based on a transition between rectangular waveguide and multiple microstrip lines," *IEEE Trans. Microw. Theory Techn.*, vol. 61, no. 7, pp. 2585–2593, Jul. 2013.
[29] L. Guo, J. Li, W. Huang, H. Shao, and T. Ba, "A compact four-way power combiner," *IEEE Microw. Wireless Compon. Lett.*, vol. 27, no. 3, pp. 239–241, Mar. 2017.
[30] L. Guo *et al.*, "A waveguide magic-T with coplanar arms for high-power solid-state power combining," *IEEE Trans. Microw. Theory Techn.*, vol. 65, no. 8, pp. 2942–2952, Aug. 2017.
[31] F. F. He, K. Wu, W. Hong, L. Han, and X. Chen, "A planar magic-T structure using substrate integrated circuits concept and its mixer applications," *IEEE Trans. Microw. Theory Techn.*, vol. 59, no. 1, pp. 72–79, Jan. 2011.
[32] F. Ardemagni, "An optimized L-band eight-way Gysel power divider-combiner," *IEEE Trans. Microw. Theory Techn.*, vol. MTT-31, no. 6, pp. 491–495, Jun. 1983.
[33] C. Chang *et al.*, "Enhanced window breakdown dynamics in a nanosecond microwave tail pulse," *Appl. Phys. Lett.*, vol. 104, no. 25, pp. 253504–253505, Jun. 2014.
[34] C. Chang, G. Liu, C. Tang, C. Chen, and J. Fang, "Review of recent theories and experiments for improving high-power microwave window breakdown thresholds," *Phys. Plasmas*, vol. 18, no. 5, p. 055702, Apr. 2011.
[35] C. Chang, *Breakdown Physics in High-Power Microwave System*. Beijing, China: Science Press, 2016.
[36] J.-W. B. Bragg, W. W. Sullivan, III, D. Mauch, A. A. Neuber, and J. C. Dickens, "All solid-state high power microwave source with high repetition frequency," *Rev. Sci. Instrum.*, vol. 84, no. 5, p. 054703, 2013.
[37] M. B. Walls, A. Fierro, J. Dickens, J. Mankowski, and A. Neuber, "A variable resistance thyristor-type switch modeling technique," *IEEE Trans. Plasma Sci.*, vol. 44, no. 9, pp. 1842–1846, Sep. 2016.
[38] Y. Wu, Y. Liu, Y. Zhang, J. Gao, and H. Zhou, "A dual band unequal wilkinson power divider without reactive components," *IEEE Trans. Microw. Theory Techn.*, vol. 57, no. 1, pp. 216–222, Jan. 2009.
[39] Y. Wu, Y. Liu, Q. Xue, S. Li, and C. Yu, "Analytical design method of multiway dual-band planar power dividers with arbitrary power division," *IEEE Trans. Microw. Theory Techn.*, vol. 58, no. 12, pp. 3832–3841, Dec. 2010.
[40] Y. Wu, Y. Liu, and Q. Xue, "An analytical approach for a novel coupled-line dual-band Wilkinson power divider," *IEEE Trans. Microw. Theory Techn.*, vol. 59, no. 2, pp. 286–294, Feb. 2011.
[41] Y. Wu, Y. Liu, and S. Li, "A modified Gysel power divider of arbitrary power ratio and real terminated impedances," *IEEE Microw. Wireless Compon. Lett.*, vol. 21, no. 11, pp. 601–603, Nov. 2011.

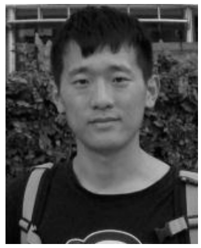

LETIAN GUO was born in Shandong, China, in 1990. He received the B.S. degree in electrical engineering from Xi'an Jiaotong University, Xi'an, China, in 2012, and the M.S. degree in electromagnetic field and microwave technology from the Northwest Institute of Nuclear Technology, Xi'an, in 2015. He has been with the Northwest Institute of Nuclear Technology since 2012. His current research interests include the microwave passive devices.

JIAWEI LI was born in Liaoning, China, in 1985. He received the B.S. degree in electrical engineering from the University of Science and Technology of China, Hefei, China, in 2008, and the M.S. degree in electromagnetic field and microwave technology from the Northwest Institute of Nuclear Technology, Xi'an, China, in 2011. He has been with the Northwest Institute of Nuclear Technology since 2008. His current research interests include high-power microwave transmission and radiation.

WENHUA HUANG was born in Jiangxi, China, in 1968. He received the B.S. degree in radio physics from Lanzhou University, Lanzhou, China, in 1991, the M.S. degree in optical engineering from the National University of Defense Technology, Changsha, China, in 2000, and the Ph.D. degree in electronic physics from Xi'an Jiaotong University, Xi'an, China, in 2011. He has been with the Northwest Institute of Nuclear Technology since 1991, where he is currently a Full Professor. His current research interests include high-power microwave and radiation technology. He was a recipient of many awards and prizes from the Chinese Government.

HAO SHAO was born in Henan, China, in 1971. He received the B.S. degree in physics from Jiaotong University, Xi'an, China, in 1994, and the M.S. degree in electromagnetic field and microwave technology and the Ph.D. degree in nuclear science and technology from the Northwest Institute of Nuclear Technology, Xi'an, in 2000 and 2005, respectively. He has been with the Northwest Institute of Nuclear Technology since 1994. His current research interests include transmission and radiation technology and high-power microwave sources

TAO BA was born in Shandong, China, in 1982. He received the M.S. degree in electromagnetic field and microwave technology, and the Ph.D. degree in nuclear science and technology from the Northwest Institute of Nuclear Technology, Xi'an, in 2013. He has been with the Northwest Institute of Nuclear Technology since 2006. His current research interests include microwave effects and diagnostics.